MICROSTRUCTURAL ASPECTS OF THERMAL OXIDATION OF THIN FILMS DEPOSITED BY EB-PVD ON STAINLESS STEEL SUBSTRATE

Laurentiu Florin MOSINOIU[1], Cristian PREDESCU[2], Radu Robert PITICESCU[1], Mircea CORBAN[1], Arcadii SOBETKII[1], Andreea GHITA[1], Albert Ioan TUDOR[1]

Protective coatings applied to components in the hot section of gas turbines using the electron beam physical vapour deposition method, EB-PVD, allow higher operating temperatures of components in this section and thus higher turbine operating efficiency. This paper presents the structural changes occurring as a result of the heat treatment applied for: 4h at 800 ^0C, to ceramic oxide thin film deposition such as: Al_2O_3 and oxide multilayers of: Al_2O_3+ZrO_2 doped with OPR - (rare earth oxides – CeO_2; Nd_2O_3; La_2O_3; GdO_3), respectively, with controlled layer thickness and uniform particle distribution capacity on 304L stainless steel substrate. SEM-EDAX analysis after this heat treatment applied to the material samples showed the appearance of microcracks in the deposited ceramic film layers, most likely caused by different thermal expansion coefficients between metal and ceramic. A thermal analysis (DSG, TG) was carried out on samples of these types of materials, the results obtained did not reveal any transformations (exothermic, endothermic) in the temperature range: 20-1400 ^0C, the materials tested being thermally stable.

Keywords: heat treatment, stainless steel, ceramic materials, EB-PVD, characterization

1. Introduction

Stainless steels are passive alloys, due to their chemical composition they form a thin oxide layer that inhibits the dissolution of the metal in corrosive environments [1]. The physical, mechanical and anti-corrosive properties of the alloy are closely related to its microstructure, where two phases (austenite, ferrite or both) occur [2-3]. Due to their unique properties, including adaptation to changes in solution salinity and pH level, these alloys are widely used in application areas such as heat exchangers [4-5].

Thermal barrier coating (TBC) systems are widely used in modern gas turbine engines to reduce the metal surface temperature in the combustion section

[1] National R&D Institute for Nonferrous and Rare Metals – IMNR, Pantelimon, Romania, corresponding author's e-mail: flaurentiu94@yahoo.com
[2] Prof., Dept. of Ecometallurgy and Materials Processing, University POLITEHNICA of Bucharest, Romania

and turbine hardware. Engines for both aviation jet propulsion and industrial power generation have taken advantage of the benefits of this technology to meet increasing demands for fuel efficiency, lower NO_x emissions and higher power. Engine components exposed to extreme temperatures are the combustion chamber and the initial engine components. rotor blades and high-pressure nozzle guide vanes. Metal temperature drops of up to 165oC are possible when using TBCs in conjunction with external film cooling and air cooling of internal components. [6-9]. Gas turbine engines applied to aircraft are engines whose efficiency and basic power are directly related to the gas temperature in the turbine section. Therefore, great efforts to improve turbine operating temperature have been made in recent decades.

These efforts mainly focus on the fabrication of turbine blades from single crystal superalloys provided with internal holes and channels for cooling, optimization of alloy compositions to achieve properties such as high creep resistance and high temperature oxidation resistance, and deposition of thermal barrier coatings (TBC) on the blades to isolate the metal components from the hot gas stream [10-14]. However, compared to applications for TBCs, the improvements obtained by adjusting alloy composition and cooling technology are quite limited. Typical TBCs consist of three main layers: the ceramic capping layer that confers a thermally protective thermal effect, the Ni alloy bonding layer (BC) that provides protection against oxidation as well as protection against mismatch between the top layer and the Ni-based superalloy substrate, and finally the intermediate layer (interlayer). The final thermally grown oxide (TGO)- Al_2O_3 layer between the capping layer and the alloy. Electron Beam Physical Vapor Deposition (EB-PVD) is a high vacuum thermal coating process in which a focused high energy electron beam is directed towards a material (metal, ceramic) to be evaporated inside a vacuum chamber. The evaporating material is then condensed on the surface of a substrate or component to form the film layer [32]. The distinct advantages of this approach are high deposition purity, increased surface area, precise film thickness, in situ growth monitoring and smoothness control [33]. In addition to the associated advantages, the aforementioned technique has proven its ability to deposit alloys, as demonstrated by Almeida et al [33] with their study of MCrAlY film fabrication. On an industrial scale, EB-PVD has been widely used for coating materials, including stainless steel-type materials [32-33].

The aim of this work is to study the thermal oxidation process for ceramic thin films deposited on stainless steel metal substrates using EB-PVD. The present work, based on the literature review is the EB-PVD process reported for the formation of NiCrAlY-Al2O3 and ZrO2 films doped with rare earth oxides OPR. The objective of the study is to evaluate and how the EB-PVD Al_2O_3 and ZrO_2 top layers doped with OPR behave at 800 ^{0}C for 4h.

2. Materials and methods

The 304L steel substrate in the form of plates with dimensions of 30x50x2 mm and 57x57x2 mm respectively, and thickness of 2 mm, were previously cleaned and degreased in organic solutions. The thus cleaned substrate plates were then fixed in a device, which is coupled to a rotating mechanism with which the e-beam installation is equipped, and which rotates at 20 rpm during the coating process. The raw materials for the deposition of the multilayer coatings were: NiCrAlY(Amperit 413), commercial Al_2O_3 powder (Amperit 740.002, max 99, 5 wt% Al_2O_3) and ZrO2 powder doped with rare earth oxides-OPR obtained by a hydrothermal synthesis process at temperatures of: 250°C and pressures of: 40 atm. The deposition was performed on a 304L stainless steel substrate in a fully automated EB-PVD advanced vacuum deposition system (Torr Inc, USA).

The electron beam controlled evaporation system consists of a stainless steel vacuum chamber with dimensions: 1500 x 1500 x 1650 mm (volume approx. 3m3), provided with process viewing holes. The chamber and front door are permanently water cooled. The water-cooled crucibles have been loaded with the above-mentioned materials to be evaporated. The deposition of the multilayer film was achieved using 2 electron guns of 10 kW each placed inside the vacuum chamber. The deposition thickness was continuously controlled using an electronic balance equipped with a quartz sensor. The substrate was heated to a temperature of approx. 800 °C using a radiant heater located behind the substrates to ensure good adhesion of the deposited films (metallic, ceramic), the working vacuum inside the enclosure being (approx. 10^{-6} Torr) and the deposition rate being approx. 0.8-2 A/s.

The oxidation heat treatment applied to the material samples was carried out in a furnace type: HTF1800, at 800 ^{0} C, for 4h. Multilayer deposition was carried out on 304L stainless steel substrates. Several types of deposition were carried out, using NiCrAlY metal alloy as a bonding layer, an intermediate layer Al_2O_3 and ZrO_2 doped with OPR having thicknesses of: 9-15µm. The samples after the oxidation heat treatment were investigated by SEM electron microscopy with a Quanta 250 (FEI) high resolution scanning electron microscope equipped with XT Microscope server software and an energy dispersive X-ray spectrometer consisting of an ELEMENT Silicon fixed detector. Analyses were performed both on the surface of the samples for the study of the microstructure of multilayer deposits and in cross-section for the study of deposited layer films.

In the case of surface analyses, the samples were fixed directly on the C-band and for cross-sectional analyses, the samples were embedded in epoxy resin, then sanded and polished. The study of thermal analysis by Differential scanning calorimetry- thermogravimetry analysis DSC-TG method of sample mass as a function of temperature when heating or cooling was also carried out.

3. Results and discussion

The investigation in Fig. 1 shows the cross-sectional micrographs of 304L stainless steel coated with the two layers: NiCrAlY and Al_2O_3 bond coatings. The deposited layers are continuous, without the appearance of pores or microcracks typical of the EB-PVD process.

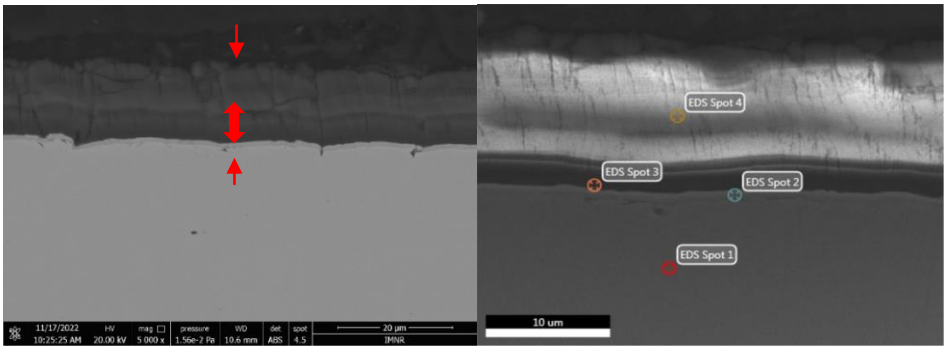

Fig.1 SEM micrograph - cross section of EB-PVD - NiCrAlY and Al_2O_3 deposition sample on 304L stainless steel substrate - thermally non-oxidized and EDS analysis with selected spots

The chemical composition of each layer was estimated by EDS analysis on the selected areas highlighted in Fig.2. The results presented in the figure show that most of the elements contained in the powder evaporated by the EB-PVD process are found on the deposition made on the 304L stainless steel substrate.

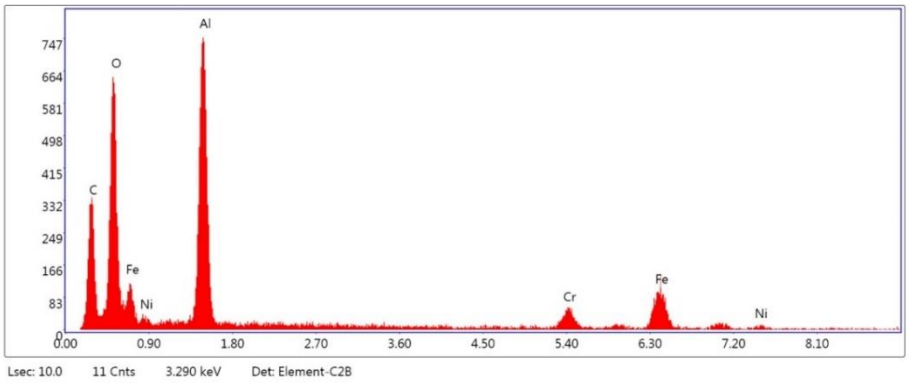

Fig. 2 Qualitative EDS analysis on the sample surface section - Acros and Al_2O_3 deposited by EB-PVD process on 304L stainless steel substrate performed in point 1

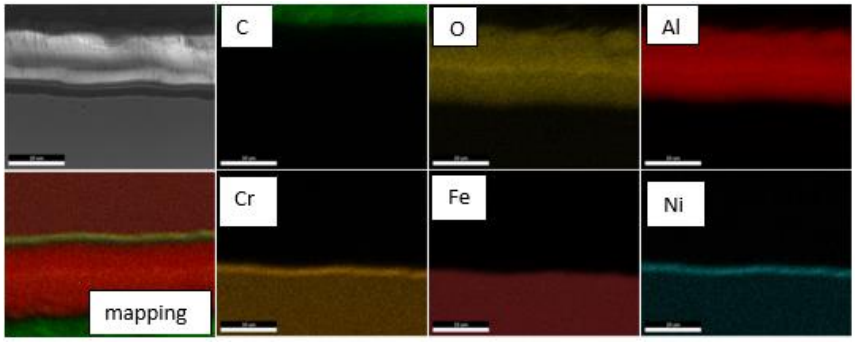

Fig.3 EDS mapping analysis of thermally non-oxidized NiCrAlY and Al_2O_3 sample

The investigation in Fig.4 shows the SEM micrograph in transverse section of deposition by EB-PVD process with NiCrAlY, Al_2O_3 - and ZrO_2 doped with rare earth oxides on 304L stainless steel substrate before thermal oxidation.

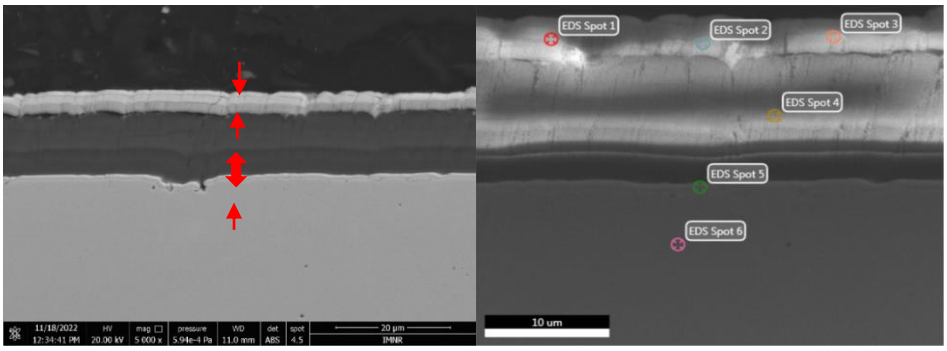

Fig.4 SEM cross-sectional micrograph of NiCrAlY, Al_2O_3 on stainless steel substrate and OPR doped ZrO_2 on thermally non-oxidized 304L stainless steel substrate and selected spots for EDS analysis.

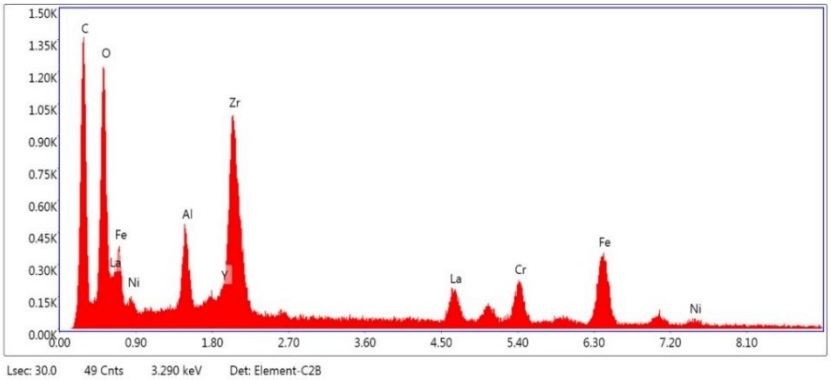

Fig.5 Qualitative EDS analysis on the cross-sectional surface of the samples - acros and oxide multilayers - (Al_2O_3 and ZrO_2 - OPR) deposited by EB-PVD process on 304L stainless steel substrate performed in point 1

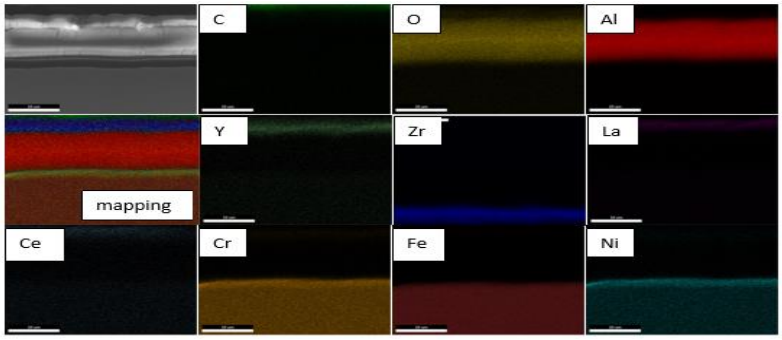

Fig. 6 EDS mapping analysis of NiCrAlY, Al_2O_3 and ZrO2 doped with thermally non-oxidized OPR.

The investigation in Fig. 7 shows the SEM morphological appearance of the deposition surface by EB-PVD – Al_2O_3 process on 304L stainless steel substrate after thermal oxidation process.

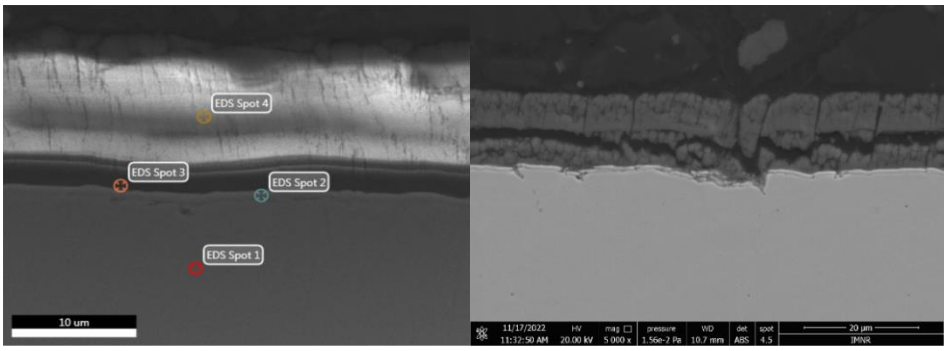

Fig. 7 SEM micrograph of cross section of EB-PVD deposition of thin films (layers) of NiCrAlY and Al_2O_3 on 304L stainless steel substrate and selected spots for EDS analysis - thermally oxidized sample.

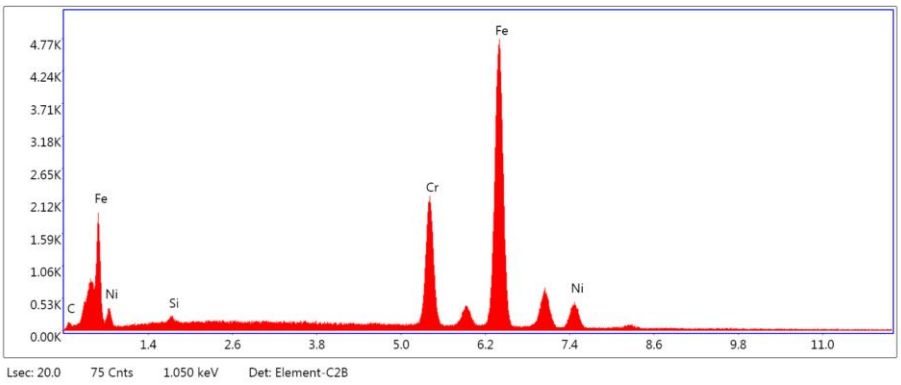

Fig.8 . Qualitative EDS analysis on the cross-sectional surface of the thermally oxidized sample performed in point 1

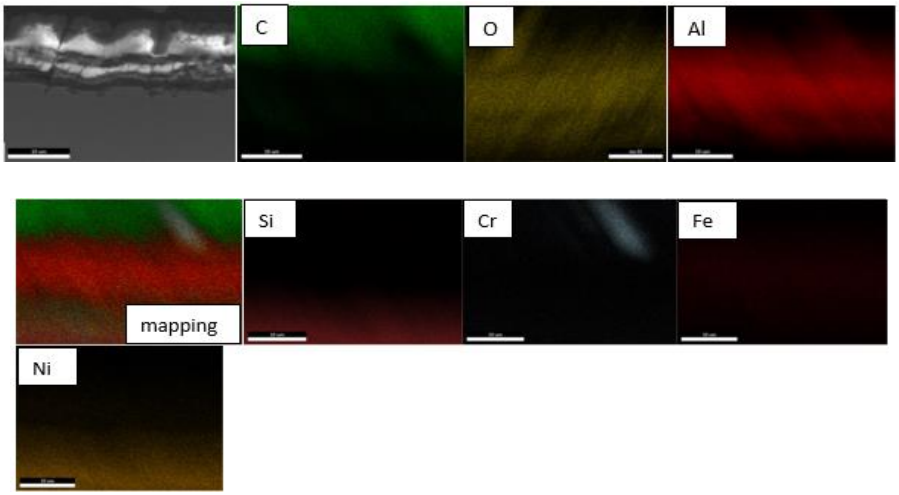

Fig. 9 EDS mapping analysis of thermally oxidized NiCrAlY and Al_2O_3 sample

The investigation in Fig.10 shows the SEM morphological appearance of the deposition surface by EB-PVD process with NiCrAlY, Al_2O_3 and ZrO_2 doped with rare earth oxides on 304L stainless steel substrate after thermal oxidation process.

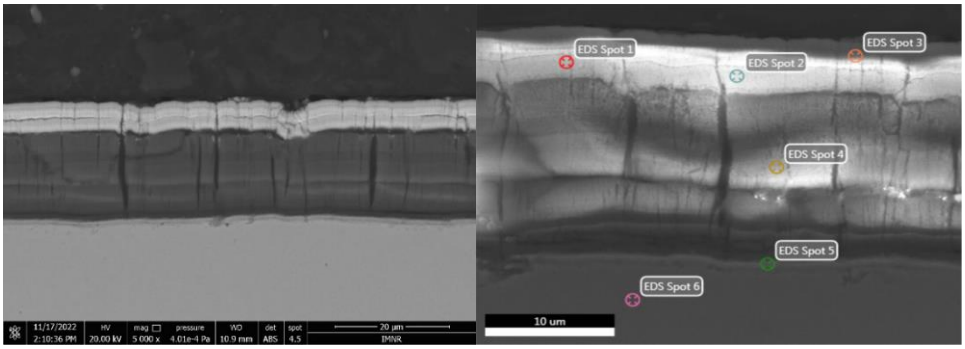

Fig.10 SEM micrograph of cross section of EB-PVD deposition of thin films (layers) of: NiCrAlY, Al_2O_3 and ZrO_2 doped with OPR on 304L stainless steel substrate and selected spots for EDS analysis - thermally oxidized sample.

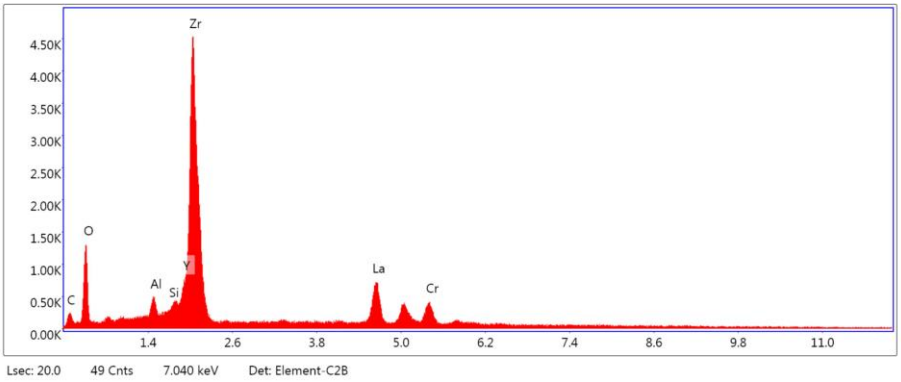

Fig. 11 Qualitative EDS analysis on the cross-sectional surface of thermally oxidized sample P1 performed in point 1.

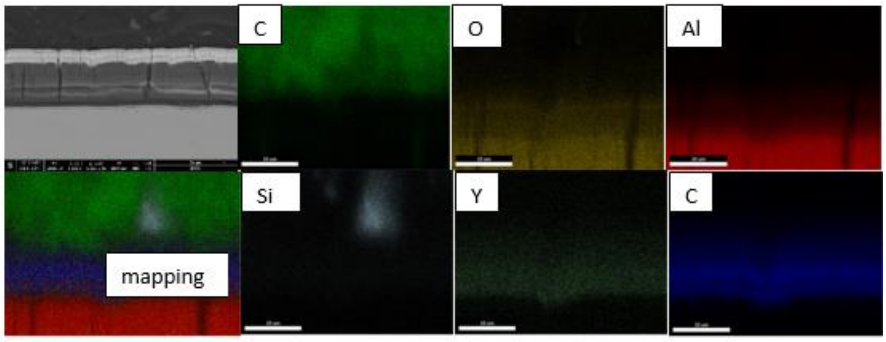

Fig. 12 EDS mapping analysis of thermally oxidized OPR-doped NiCrAlY, Al_2O_3 and ZrO2.

Thermal analysis was performed on both samples with: NiCrAlY- Al_2O_3 deposited on 304L stainless steel substrate and on: NiCrAlY- Al_2O_3- ZrO_2 doped with OPR - rare earth oxides deposited on 304L stainless steel substrate using SETSYS EVOLUTION equipment, Setaram -France. The samples were subjected to a controlled heating and cooling process. The samples were subjected to a thermal heating process in the temperature range 20°C - 1350°C, with a heating rate of 10°C/minute, and cooling to 20°C was performed at a rate of 20°C/minute. The heating and cooling operations were carried out in Ar atmosphere. The curves shown in the figures below highlight the phase transformations (blue curve) and mass loss (green curve) that occur in the samples analyzed during the heating steps.

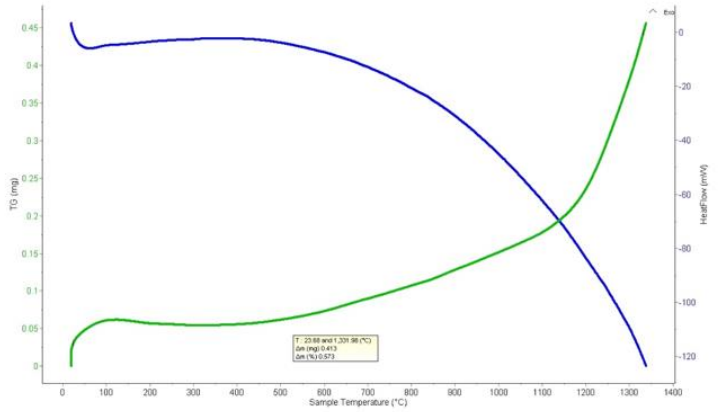

Fig. 13. Thermogram of NiCrAlY and Al_2O_3 sample deposited EB-PVD on 304L stainless steel substrate.

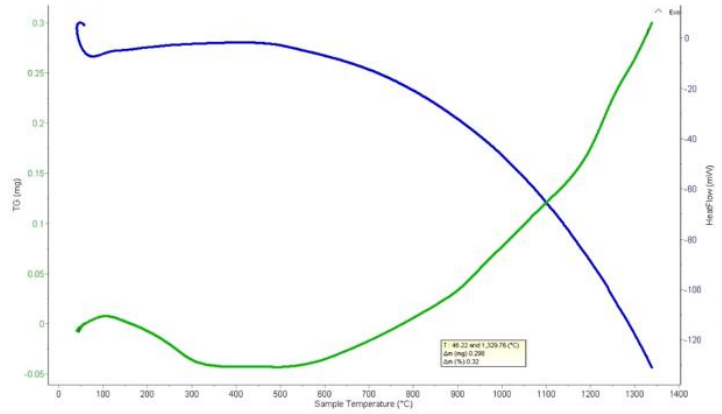

Fig. 14. Thermogram of NiCrAlY, Al_2O_3 and ZrO_2 sample doped with EB-PVD deposited OPR on 304L stainless steel substrat.

The DSC-TG analysis indicates that no phase transformations occur.

4. Conclusion

The deposited layers are continuous and adherent in the form of columnar crystals grown perpendicular to the substrate surface. This columnar growth is specific to EB-PVD deposition, and the deposition follows the contour of the stainless steel substrate surface.

The results obtained by comparing the samples before and after the thermal oxidation process show microstructure changes in the area between Al_2O_3 and ZrO_2 doped with OPR. After the heat treatment microcracks appeared in the

oxide thin films. These microcracks may be caused by different expansion/contraction stresses between the ceramic oxides and the metal substrate.

It was also observed that in the case of the sample with NiCrAlY- Al_2O_3 deposits on 304L stainless steel substrate, the microcracks are more accentuated, extended, even appearing as a gap, unlike the sample with NiCrAlY- Al_2O_3 – ZrO_2 deposits doped with OPR, where they are more pronounced. Work will continue to optimise adhesion and resistance to thermal oxidation.

Acknowledgments

This work has been funded by the European Social Fund from the Sectoral Operational Programme Human Capital 2014-2020, through the Financial Agreement with the title "Training of PhD students and postdoctoral researchers in order to acquire applied research skills - SMART", Contract no. 13530/16.06.2022 - SMIS code: 153734".

R E F E R E N C ES

[1]. *Landoulsi J., Genet M.J., Richard C., El Kirat K., Pulvin S., Rouxhet P.G*. Evolution of the passive film and organic constituents at the surface of stainless steel immersed in fresh water. J. Colloid InterfaceSci. 2008, pp. 278–289.

[2]. *Tylek I., Kuchta K.* Mechanical properties of structural stainless steels. Civil Eng, 2014, pp. 59-80.

[3]. *Corradi M., Di Schino A., Borri A., Rufini R.* A review of the use of stainless steel for masonry repair andreinforcement. Constr. Build. Mater, 2018181, pp. 335-346.

[4]. *Bowden D., Krysiak Y., Palatinus L., Tsivoulas D., Plana-Ruiz S., Sarakinou E., Kolb U., Stewart D., Preuss M.* A high-strength silicide phase in a stainless steel alloy designed for wear-resistant applications. Nat. Commun, ,2018, pp. 9:1–10.

[5]. *Trzaskowska P.A., Kuźmińska A., Butruk-Raszeja B., Rybak E., Ciach T.* Electropolymerized hydrophilic coating on stainless steel for biomedical applications. Colloids Surf. B, 2018, pp. 167:499–508.

[6]. *S.M. Meier, D.K. Gupta, and K.D. Sheffler, Ceramic* Thermal Barrier Coatings for Commercial Gas Turbine Engines, J. Metal, 1991, p 50-53.

[7]. *A. Maricocchi, A. Barz, and D. Wortman*, PVD TBC Experience on GE Aircraft Engines, Thermal Barrier Coating Workshop, NASA Lewis Research Center, Cleveland, OH, March 27-29, NASA Conference Publication, 1995, pp. 79-90.

[8]. *D.V. Rigney, R. Viguie, D.J. Wortman, and D.W. Skelly*, PVD Thermal Barrier Coating Applications and Process Development for Aircraft Engines, J. Therm. Spray Technol., 1997, pp. 167 .

[9]. *D. Zhu, J.A. Nesbitt, C.A. Barrett, T.R. McCue, and R.A. Miller*, Furnace Cyclic Oxidation Behavior of Multicomponent Low Conductivity Thermal Barrier Coatings, J. Therm. Spray Technol., 2004, 13(1), pp. 84-92.

[10]. *Gleeson, B.*, Thermal Barrier Coatings for Aeroengine Applications. J. Propul. Power 2006, pp. 375-383.

[11]. *Clarke, D. R.,* Materials selection guidelines for low thermal conductivity thermal barrier coatings. Surf. Coat. Technol. 2003, pp. 163–164, 67-74.
[12]. *Evans, A. G.; Clarke, D. R.; Levi, C. G.,* The influence of oxides on the performance of advanced gas turbines. J. Eur. Ceram. Soc, 2008, pp. 1405-1419.
[13]. *Evans, A. G.; Mumm, D. R.; Hutchinson, J. W.; Meier, G. H.; Pettit, F. S.,* Mechanisms controlling the durability of thermal barrier coatings. Prog. Mater Sci. 2001, pp. 505-553.
[14]. *Mumm, D. R.; Evans, A. G.,* On the role of imperfections in the failure of a thermal barrier coating made by electron beam deposition. Acta Mater. 2000, pp. 1815-1827.
[15]. *Li W.-Y., Liao H., Douchy G., Coddet C*. Optimal design of a cold spray nozzle by numerical analysis of particle velocity and experimental validation with 316L stainless steel powder. Mater. Des. 2007, pp. 2129–2137.
[16]. *Wanjara P., Brochu M., Jahazi M.* Electron beam freeforming of stainless steel using solid wire feed. Mater. Des. 2007, pp. 2278–2286.
[17]. *Sobetkii. A., Mosinoiu L., Paraschiv A., Corban M.,* Microstructural aspects of the protective ceramic coatings applied on the surfaces of refractory alloys produced by additive manufacturing, 2020, pp. 33
[18]. *Sahoo B., Schlage K., Major J., Von Hörsten U., Keune W., Wende H., Röhlsberger R*. Preparation and characterization of ultrathin stainless steel films. AIP Conf. Proc. 2011, pp. 1347:57–60.
[19]. *Nomura K., Iio S., Ujihira Y., Terai T.* DCEMS study of thin stainless steel films deposited by RF sputtering of AISI316L. AIP Conf. Proc. 2005, pp. 765:108–113.
[20]. *De Baerdemaeker J., Van Hoecke T., Van Petegem S., Segers D., Bauer-Kugelmann W., Sperr P., Terwagne G.* Investigation of stainless steel films sputtered on glass. Mater. Sci., 2001, pp. 363:496–498.
[21]. *Kraack M., Boehni H., Muster W., Patscheider J.* Influence of molybdenum on the corrosion properties of stainless steel films. Surf. Coat. Technol, 1994, pp. 68–69:541–545.
[22]. *Eymer J.P*. On the hyperfine field of bcc 304 L stainless steel films. J. Phys. IV France. 1992, pp. 11-215.
[23]. Godbole M.J., Pedraza A.J., Allard L.F., Geesey G. Characterization of sputter-deposited 316L stainless steel films. J. Mater. Sci., 1992, pp. 5585–5590.
[24]. *Pedraza A.J., Godbole M.J., Bremer P.J., Avci R., Drake B., Geesey G.G*. Stability in aqueous media of 316L stainless steel films deposited on internal reflection elements,1993, pp.47:161–166.
[25]. *Song Y.S., Lee J.H., Lee K.H., Lee D.Y.* Corrosion properties of N-doped austenitic stainless steel films prepared by IBAD. Surf. Coat. Technol., 2005, pp. 195:227–233.
[26]. *Nomura K., Yamada Y., Tomita R., Yajima T., Shimizu K., Mashlan M.* CEMS study of stainless steel films deposited by pulsed laser ablation of AISI316. Czech J. Phys., 2005, pp. 845–852.
[27]. Koinkar V.N., Chaudhari S.M., Kanetkar S.M., Ogale S.B. Deposition of stainless steel film using pulsed laser evaporation. Thin Solid Films, 1989, pp. 335–342.
[28]. 29. Singh J., Wolfe D.E. Review Nano and macro-structured component fabrication by electron beam-physical vapor deposition (EB-PVD) J. Mater. Sci. 2005, pp. 40-26.
[29]. *Arunkumar P., Aarthi U., Sribalaji M., Mukherjee B., Keshri A.K., Tanveer W.H., Cha S.-W., Babu K.S.* Deposition rate dependent phase/mechanical property evolution in zirconia and ceria-zirconia thin film by EB-PVD technique. J. Alloys Compd., 2018, pp. 765:418–427.
[30]. *De Almeida D.S., da Silva C.R.M., do Carmo* M. Ni Al alloy coating deposition by electron beam physical vapour deposition; Proceedings of the 17th Brazilian Congress of Engineering and Materials Science, 2006, pp. 15-19.

[31]. *Singh J., Wolfe D., Quli F.* IMAST Quarterly. Pennsylvania State University; University Park, PA, USA: Electron beam-physical vapor deposition technology: Present and future applications, 2000, pp. 3–6.
[32]. *Nam Y., Ju Y.S.* A comparative study of the morphology and wetting characteristics of micro/nanostructured Cu surfaces for phase change heat transfer applications. J. Adhes. Sci. Technol., 2013, pp. 27:2163–2176.
[33]. *Cai Y., Chang W., Luo X., Sousa A.M.L., Lau K.H.A., Qin Y.* Superhydrophobic structures on 316L stainless steel surfaces machined by nanosecond pulsed laser. Precis. Eng.